Analytical modeling of steady-state filtration process in an automatic self-cleaning filter

Martine Meireles, Marc Prat, Guillaume Estachy

Analytical modeling of steady-state filtration process in an automatic self-cleaning filter

M. Meireles[a,b,*], *M. Prat*[c,d], *G. Estachy*[e]

[a] *Université de Toulouse, INPT, UPS, Laboratoire de Génie Chimique, 118 Route de Narbonne, F-31062 Toulouse, France*
[b] *CNRS, UMR 5503, F-31062 Toulouse, France*
[c] *Université de Toulouse, INPT, UPS, Institut de Mécanique des Fluides de Toulouse, Avenue Camille Soula, F-31400 Toulouse, France*
[d] *CNRS, UMR 5502, F-31400 Toulouse, France*
[e] *Alfa Laval Moatti SAS, 10 Rue du Maréchal de Lattre de Tassigny, 78997 Elancourt Cedex, France*

A B S T R A C T

An automatic self-cleaning filter is a semi continuous machine operated for the removal of particles from a fluid. Technically, a distributor driven by a hydraulic motor rotates at regular intervals to feed the slurry to the inlet chambers of N segmented elements horizontally stacked over the distributor and back-flushes the last chamber. In this work a practical computationally-affordable model has been developed to describe the distribution of flow rate in the different sectors of a disc-type element and to demonstrate the effect of parameters, such as backflushing time or pollution concentration, accounting for particle clogging and periodic operation conditions for perfect and imperfect efficiency of the cleaning by back-flushing. The key results are the prediction of the time of clogging, as well as a numerical tool to optimize critical back-flushing time and pollution concentration.

Keywords:
Filtration
Hydrodynamic
Self-cleaning
Multiscale modeling

1. Introduction

Fully automatic self-cleaning filters have been used for decades in applications wherever suspended solids need to be removed from a pressurized water stream. They are mainly used in closed loop industrial systems, on deep-sea oil platforms and on large ships for hydraulic systems. Marine engines operate in most severe environments, running nearly 24 h a day and under extreme loads. It is very important that the engines and hydraulic systems operate efficiently and require little to no downtime. For automotive engines, oil change is a routinely task, but for marine engines, operators have to face the potential for an oil spill, the difficulty to dispose of the used motor oil and the cost associated with these types of changes. For this purpose, compact automatic self-cleaning filters have been developed by several worldwide companies to be operated on large marine engines to remove particles from lube oil in diesel engine of ships. An interesting and distinguishing feature of an automatic filter is that the backflushing occurs without interruption of the flow downstream of the filter. For this end a specific design is needed which allows the periodical rotation of filtration chambers inside the filter housing. Such a design allows to simultaneously feed some chambers while others are backflushed to remove the accumulated particles from the filter. The technical scheme of a compact automatic self-cleaning filter is presented in Fig. 1. It is composed of horizontally stacked disc-type elements mounted over a distributor. Each disc-type

* Corresponding author at: Université de Toulouse, INPT, UPS, Laboratoire de Génie Chimique, 118, route de Narbonne, 31062 Toulouse, France. Tel.: +33 561558162.
E-mail address: meireles@chimie.ups-tlse.fr (M. Meireles).
http://dx.doi.org/10.1016/j.cherd.2015.04.030

List of symbols:

A_s	screen area A_s
C	concentration of solid particles (g m^{-3})
d_h	screen hole size (m)
d_p	particle equivalent diameter (m)
d_{moy}	average particle size calculated from the number n_i of particles of size d_i per ml of fluid (m)
$e(t)$	cake height at time t (m)
h	sector height (m)
L	sector length (m)
$M+1$	number of sectional chambers by disc-type elements
n_p	total number of particles per unit volume of apparent diameter larger than the screen hole size d_h
N	number of disc-type elements
n_o	initial number of mesh holes
$n(t)$	number of holes at time t
Q_s	volumetric liquid flow rate through the sector (m^3 s^{-1})
Q_t	volumetric flow rate entering the filter (m^3 s^{-1})
R_i	internal radii of the filter column (m)
R_e	external radii of the filter column (m)
R	filter specific resistance to viscous flow (m^{-1})
R_{ca}	cake resistance (m^{-1})
S_0	average cross-section area in the inlet chamber (m^2)
t_b	backflushing time (s)
t_c	cleaning time (s)
u	axial velocity (m s^{-1})
v	transverse velocity (m s^{-1})
u^*	adimensional axial velocity
v^*	adimensional transverse velocity
V_w	filtration velocity in the sector (m s^{-1})
U_0	average velocity in the inlet channel (m s^{-1})
x	horizontal coordinate of the sector (m)
y	vertical coordinate of the sector (m)
x^*	adimensional horizontal coordinate of the sector
y^*	adimensional vertical coordinate of the sector
α_b	free opening fraction right after backflushing
μ	dynamic viscosity (Pa s)
ρ	density (kg m^{-3})

element is made from the assembly of two frames (Fig. 2a). A disc-type element is divided into $(M+1)$ sectional sectors by ribs (Fig. 2b). The number of sectors $M+1$ is always even and of the order of 8 to 12. As outlined in Fig. 3, in a sector made from the assembly of two frames, there are an inlet chamber and two outlet chambers that we denote an upper chamber and a lower chamber. The inlet and the two outlet chambers are separated by the filter media. This chamber design thus provides a double-sided filtration area. The filtration media is usually a weave-wire screen: a simple two-dimensional square-weave with rectangular openings. By convention referring to the textile industry pores or openings of screen media are described by the term mesh. The size of the "mesh" also called the nominal filtration degree is an actual dimension of the shortest distance across the opening. It more or less corresponds to the smallest particle size which can be removed from the fluid stream.

The detailed operating principle of an automatic self-cleaning filter is described below. The system is fed with the slurry from the filter housing to the inlet chambers of N segmented disc-type elements horizontally stacked over the distributor. For each element, the M sectors are fed from the gap between the distributor and the internal side of the disc-type element (see Fig. 2a). The slurry enters the sector through the inlet chamber entrance. Upon filtration, particles build up on the surface of the two filter media located at the upper/lower side of the inlet chamber, and the clean fluid leaves the sector through the upper/lower outlet chambers. Particle accumulation causes an increased pressure drop through the sectors and therefore through each disc-type element. The liquid flow rate through the sectors of a disc-type element is maintained at a constant value by means of a displacement pump. The distributor which is driven by a hydraulic motor on the top of the filter housing continuously rotates to simultaneously feed M sectors and backflush with some amount of filtrate the $(M+1)$ sector, flushing the accumulated particles from the surface of the media (see Fig. 2a). In this way, all sectors are backflushed once per full rotation of the distributor and solids which are collected during the filtration period can be removed by backflushing after a full rotation is completed. Backflushing is common in filtration systems, e.g. (Ando et al., 2012; Bacchin et al., 2011; Benmachou et al., 2003; Berman, 1953; Duignan and Nash, 2012) to name only a few, to clean-up the filter surface periodically. The interesting and distinguishing feature of an automatic filter is that the backflushing occurs without interruption of the filtration process. Backflushing time (which corresponds to a given rotating speed) is an operating parameter of the order of 10 to 60 s. It can be specified and optimized in order to limit accumulation in the filtration chambers which depends among others on filtration media characteristics and properties of the slurry such as size distribution and shape of the particles. Even for a given application like lube oil in diesel engine of ships, fluid properties may vary from one engine to another and even with operating time for a given engine. This is the reason why, when optimizing the design (number and geometrical dimensions of elements) or the operating conditions, such as the backflushing time, engineering companies strongly rely on standardized qualification tests usually carried out with standardized fine Arizona sand with a well-characterized size distribution. Such standardized qualification tests also allow comparing automatic filters from different companies. A qualification test of a filter provides with the variation of pressure drop as a function of the time of filtration for a known concentration of particles introduced in the filter at a given volumetric rate. This allows qualifying a filter or a procedure regarding the time needed to reach a maximum pressure drop which is normally set to around 2×10^5 Pa, also called time for clogging. These tests are extensively used to compare different designs and optimize operating parameters but they are quite costly. Therefore for most engineering companies, a general objective is to develop a CPU-friendly and reliable numerical tool in order to reduce the time of design, the number of experimental trials, as well as to optimize operating conditions.

In this work a practical computationally affordable model has been developed to describe the distribution of flow rate in the different sectors of a disc-type element and to demonstrate the effect of parameters settings, such as backflushing time or pollution concentration. The aim is rather to demonstrate the effect of parameter settings than represent real cases. As will be seen further in the paper, some

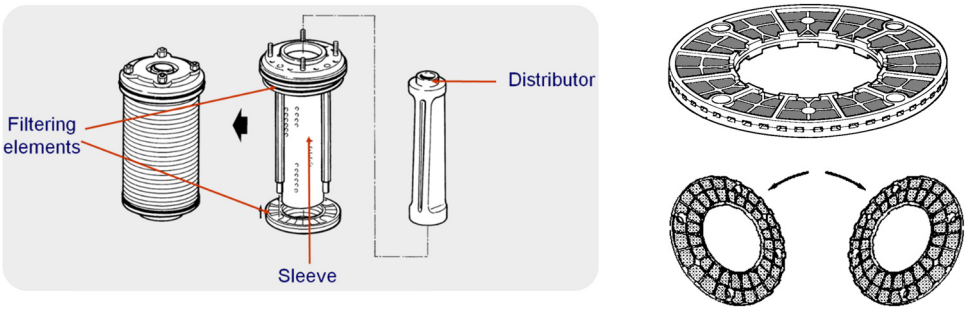

Fig. 1 – Technical scheme of an automatic filter with disk-type elements stacked over a distributor to form the filtering unit.

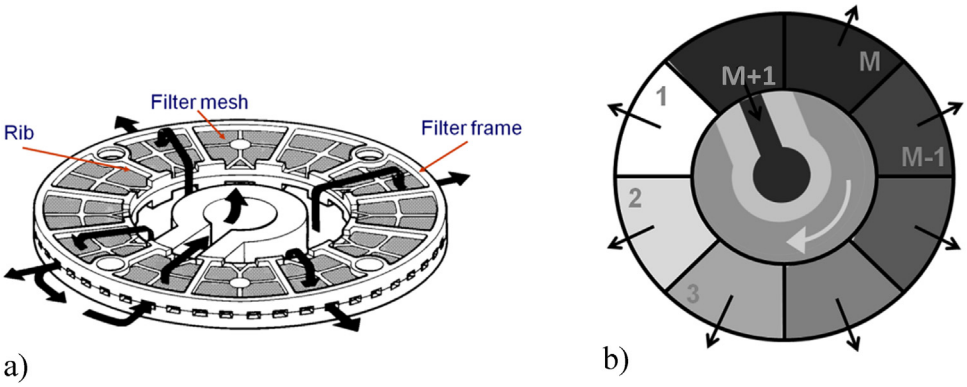

Fig. 2 – Left: scheme of the disk-type chamber composed of the assembly of two frames. Each frame is divided in $M+1$ sectional chambers by ribs. Right: scheme of the operating principle: A distributor driven by a hydraulic motor rotates at regular intervals to feed the slurry in M chambers and back flush the last chamber.

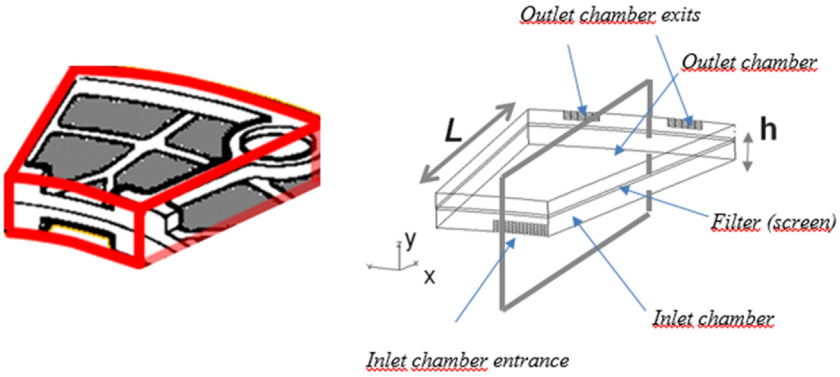

Fig. 3 – Left: design of sector geometry, right: schematic representation of half and inlet and half and outlet chambers. L is the length of the sector and h the half width, x and y are the coordinates. Note that only half of inlet chamber (outlet chamber respectively) is shown. Hence each inlet chamber (outlet chamber respectively) in the system is bordered by two filtration screens. The plane limited by the dashed line is the plane corresponding approximately to the 2D model.

geometrical data are taken from the design of a real Alfa Moatti filter for the sole purpose of model development (see Table 1 for instance). These inputs can easily be replaced with alternative data without affecting the generality of the methodology developed here. Also a comparison between the calculation of time for clogging and experimental test of an automatic self-cleaning filter will be provided. The problem requires a multi-scale approach from the filter media micro-scale up to the macro-scale of the automatic self-cleaning filter, which implies the consideration of two intermediate scales (chambers of a sector and disc-type element). It should also account for the periodicity of filtration and backflushing in the $M+1$ sectors of a disc-type element due to the continuous rotation of the filter, noting that after one fill rotation, filtration occurs at a steady state. The objective is not a detailed modeling but a simplified CPU friendly approach useful to gain insights into the influence of main parameters. For this end, we shall use a simplified model of the flow (in the absence of

Table 1 – Geometrical data for Alfa-Laval Moatti Filter 150 and physical characteristics of Alla-Laval A03 screen media.

Class size (μm)	>6	>8	>10	>14	>17	>4	>20	>22
Number of particles for 20 ml	10,4131	46,452	124,845	8424	4058	28,736	2058	1391
Class size (μm)	>28	>30	>35	>40	>45	>25	>50	>70
Number of particles for 20 ml	347	219	83	36	15	676	8	3

particles) derived from cross sectional averaging of the Navier Stokes equations in a sector using similarity solutions (Section 2). Clogging scenarii are studied in Section 3 based on standard models and experimental evolution of pressure drop. In Section 4, a complete model for stationary regime is developed and used for studying the influence of backflushing time and pollution concentration on the flow distribution in the different sectors and to calculate the pressure drop increase of a filter.

2. Flow characteristics in the filtration chambers

We begin the analysis by assuming that the main contribution to the pressure drop is due to the flow within the filtration chambers. All other contributions such as pressure drop in the distributor or in the filter housing are neglected. Consistently with this assumption, we further assume that the flow through each disc-type element is the same whatever the position of the element in the stack. These assumptions imply that,

$$\Delta P_f(t) \approx \Delta P_{ei}(t) \quad 1 \le i \le N \tag{1}$$

where N is the number of disc-type element, $\Delta P_f(t)$ and $\Delta P_{ei}(t)$ are respectively, the pressure drops across the filter composed of N elements and element i, respectively.

In this section, we study the characteristics of the flow within the inlet and upper (or lower) outlet chambers of one of the $M+1$ sectors of a disc-element. Essentially, we show that the filtration velocity in the inlet/outlet chambers can be considered as uniform along the chamber longitudinal axis for the typical conditions and geometrical dimensions encountered in an automatic filter. The analysis is based on a 1D flow model, which has been used in previous filtration studies for low to moderate filtration velocities. The main features of the model are recalled here but more details can be found in references (Gan and Allen, 1999; Koltuniewicz et al., 2004).

Due to symmetry, we consider half of a sector (in the y plane), comprising half of the inlet chamber and the upper chamber of height h (see Fig. 3). Note that h in Fig. 3 which corresponds to the half-height of the inlet chamber is also the height of the upper/lower outlet chambers. The screen thickness of the order of 0.5 micron is considered as negligible compared with h. Typical geometrical dimensions for flow chambers are 7 mm for h, and 65 mm for the length L.

There are three main features of the inlet and outlet chambers: (i) the ratio of the height to chamber length h/L is smaller than 1, (ii) the cross-sectional area increases in the x-direction, (iii) constriction effects are expected at the entrance (for the inlet chamber) and at the exit (for outlet chambers) since the fluid entrance (exit respectively) is through a fraction of the section of the inlet chamber (of the outlet chamber respectively). However, due to the relative small aspect ratio h/L, the azimuthal deformation of stream lines can be assumed to occur only over a small region of the chambers. As a result, our approach is based on the consideration of the simplified 2D geometry considering the y-axis symmetry sketched in Fig. 3 where $y=0$ at the center of the inlet channel and $y=h$ at the surface of the filter media. The flow is described using the Navier–Stokes equations expressed for this 2D geometry with the mass balance and momentum balance equations expressed in dimensionless form as:

$$\frac{\partial u^*}{\partial x^*} + \frac{\partial v^*}{\partial y^*} = 0 \tag{2}$$

$$\left(u^* \frac{\partial u^*}{\partial x^*} + v^* \frac{\partial u^*}{\partial y^*}\right) = -\frac{\partial p^*}{\partial x^*} + \frac{1}{Re_0}\left(\frac{\partial^2 u^*}{\partial x^{*2}} + \frac{\partial^2 u^*}{\partial^2 y^*}\right) \tag{3}$$

$$\left(u^* \frac{\partial v^*}{\partial x^*} + v^* \frac{\partial v^*}{\partial y^*}\right) = -\frac{\partial p^*}{\partial y^*} + \frac{1}{Re_0}\left(\frac{\partial^2 v^*}{\partial x^{*2}} + \frac{\partial^2 v^*}{\partial^2 y^*}\right) \tag{4}$$

where $x^* = \frac{x}{h}, y* = \frac{y}{h}, u^* = \frac{u}{U_0}, v^* = \frac{v}{U_0}, p^* = \frac{p}{\rho \frac{U_0^2}{U_0}} U_0$ is the average velocity in the inlet channel and $Re_0 = \frac{\rho U_0 h}{\mu}$;

ρ and μ are the fluid density and dynamic viscosity, respectively.

The above equations have to be solved in conjunctions with the boundary conditions at the surface of the filter media ($y=h$),

$$u^*(x^*, 1) = 0; \quad v^*(x^*, 1) = \frac{\langle V_w \rangle}{U_0} \tag{5}$$

In the above equation, $\langle V_w \rangle$ is the average velocity through the filter media. Due to mass conservation for a steady flow, U_0 is also the average velocity at the exit of outlet channel and is estimated as:

$$U_0 = \frac{Q_s}{S_0} \tag{6}$$

In the above equation, Q_s is the volumetric flow rate entering a sector and S_0 is the average cross-section area given by

$$S_0 = \frac{2\pi\left(R_i + \frac{R_e - R_i}{2}\right)}{M+1} h \tag{7}$$

R_i and R_e are the internal and external radii of the disc-type element, respectively.

Under the following assumptions: (i) laminar flow, (ii) quasi-uniform filtration velocity along the channel $v(x, y) = v(y)$, and (iii) $\langle V_w \rangle_y << U_0$, an analytical solution to this system can be proposed provided that $Re_w = \frac{\rho V_w h}{\mu}$ is of the order of 1, (Li et al., 1998).

According to this solution the local velocity field (u^*, v^*) is given by:

$$\frac{u^*(x^*, y^*)}{U_0} = \frac{3}{2}\frac{\langle u^* \rangle_{y*}}{U_0}\left(1 - y^{*2}\right)\left[1 - \frac{Re_w}{420}\left(2 - 7y^{*2} - 7y^{*4}\right)\right] + o\left(Re_w^2\right) \tag{8}$$

$$\frac{v^*(y^*)}{U_0} = \frac{1}{2}\frac{Re_w}{Re_0} y^*(3 - y^{*2}) + o\left(Re_w^2\right) \tag{9}$$

$\langle u^* \rangle_{y*}$ is the dimensionless average axial velocity defined by

$$\left\langle u^* \right\rangle_{y^*} = \frac{1}{h}\int_0^h u^*(x^*, y^*) dy^* \tag{10}$$

By substituting Eqs. (8) and (9) into the conservative equations and applying the averaging operator defined by Eq. (10),

one obtains, (see Gan and Allen, 1999 for the details), the following local mass balance and momentum balance equations,

$$\frac{d\langle u^*\rangle_{y*}}{dx^*} + \frac{Re_w}{Re_0} = 0 \tag{11}$$

$$\frac{81}{70}\frac{d\langle u^*\rangle^2_{y*}}{dx^*} + \frac{3}{Re_0}\left\langle u^*\right\rangle_{y*} - \frac{1}{Re_0}\frac{d\langle u*\rangle^2_{y*}}{dx^{*2}} + \frac{d\left\langle p^*\right\rangle_{y*}}{dx^*} = 0 \tag{12}$$

Eqs. (11) and (12) are used to describe the flow in both the inlet and upper outlet chambers. To couple the systems of Eqs. (11) and (12) relative to each chamber, we express the local velocity V_w through the filter media in terms of the local pressure difference according to a linear relation:

$$V_w = \frac{p_1 - p_2}{R\ \mu} \tag{13}$$

where subscripts 1 and 2 refer to inlet and upper outlet channel separated by the filter media; R is the hydraulic resistance of any type of filtration media.

According to Lin et al. (2009), the pressure drop across a mesh type filtration media can be expressed as

$$\frac{10}{Re_{sc}{}^{1.14}} = \frac{2\Delta P}{\rho(V_w/(1-A_m))^2}\frac{1}{A_m} \quad \text{with}$$

$$Re_{sc} = \frac{\rho\,(V_w/(1-A_m)\,d_h}{\mu} \tag{14}$$

where $\Delta P = p_1 - p_2$ and d_h is the size of the mesh and A_m is the open surface of the screen media or the sum of all the areas of the openings through which the fluid can pass. On the grounds, that Reynolds number, Re_{sc}, is small compared with one, one can simplify Eq. (14) as:

$$\frac{10}{Re_{sc}} \approx \frac{2\Delta P}{\rho(V_w/(1-A_m))^2}\frac{1}{A_m} \tag{15}$$

Now, combining Eqs. (13) and (15), gives us a simple relation for the hydraulic resistance of a screen filtration media:

$$R = \frac{5A_m}{(1-A_m)\,d_h} \tag{16}$$

Together with Eq. (13), Eqs. (11) and (12) governing the flow in the inlet and outlet channels are therefore, Inlet channel (subscript 1 refers to inlet channel)

$$\frac{d\left\langle u_1^*\right\rangle_y}{dx^*} + Re_0\frac{\left(p_1^* - p_2^*\right)}{hR} = 0 \tag{17}$$

$$\frac{81}{70}\frac{d\left\langle u_1^*\right\rangle^2_{y*}}{dx^*} + \frac{3}{Re_0}\left\langle u_1^*\right\rangle_y - \frac{1}{Re_0}\frac{d\left\langle u_1^*\right\rangle^2_{y^*}}{dx^{*2}} + \frac{d\left\langle p_1^*\right\rangle_y}{dx^*} = 0 \tag{18}$$

Outlet channel (subscript 2 refers to outlet channel)

$$\frac{d\left\langle u_2^*\right\rangle_y}{dx^*} + Re_0\frac{\left(p_1^* - p_2^*\right)}{hR} = 0 \tag{19}$$

$$\frac{81}{70}\frac{d\left\langle u_2^*\right\rangle^{2*}_y}{dx^*} + \frac{3}{Re_0}\left\langle u_2^*\right\rangle_y - \frac{1}{Re_0}\frac{d\left\langle u_2^*\right\rangle^2_{y^*}}{dx^{*2}} + \frac{d\left\langle p_2^*\right\rangle_{y*}}{dx^*} = 0 \tag{20}$$

The system of Eqs. (17)–(20) is solved combining a finite difference method of discretization with a Newton–Raphson method (to deal with the non-linearities and the coupled

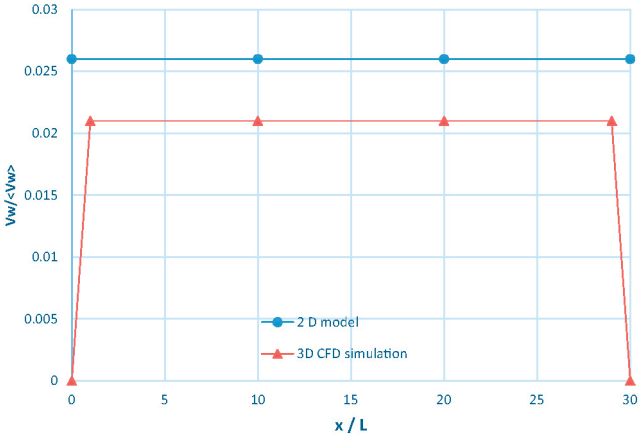

Fig. 4 – Filtration velocity along the filter screen: from top to bottom: filtration velocity calculated by the analytical model solution, filtration velocity from 3D CFD simulation in the plane limited by the dashed line in Fig. 3.

nature of the system). Details can be found in Oxarango et al. (2004). A sensitivity study of the number of grid points has been carried out, considering up to 2500 equally spaced grid points. This study indicated that a grid of 200 up to 300 points was a good trade-off between accuracy and computational time. Typically, the time for computing the flow using this 2D model is of the order of one to two seconds on a standard Linux PC. This time is to be compared with the time of 5 min needed for a direct computation using the CFD commercial software on the same platform, without mentioning the time needed for preparing the CFD computation (grid construction, etc.).

To investigate the flow characteristics in the chambers of a sector we have used geometrical and operating data of an existing automatic self-cleaning filter designed by Alfa-Moatti. The geometrical data of Alfa-Moatti150 filter are reported in Table 1. For the flow simulation the inputs are: an average inlet velocity U_0 equal to 0.2488 m s^{-1}, an average filtration $\langle V_w\rangle$ equal to 0.0268 m s^{-1}, an hydraulic resistance of the screen media R equal to 47.6×10^5 m^{-1} as given for a 25 μm absolute mesh size A03 filtration media (Alfa Laval A03 filter).

For these set of parameters, the Reynolds number Re_0 in the filtration chambers is equal to 58.5 for lube oil ($\rho = 850$ kg m^{-3}, $\mu = 2.55\times10^{-2}$ Pa s at 25 °C) which corresponds to a laminar flow whereas the Reynolds number Re_w of the flow through the screen is equal to 6. This does not entirely meet the requirement Re_w of the order of 1 but is sufficiently small to obtain reasonably good results.

In order to validate the 2D-simplified model, comparisons with three dimensional CFD computations have been carrying out using commercial software (Fluent, ANSYS). On the whole the agreement between our model and the CFD direct simulation is very good. A representative example of the results, Fig. 4 shows ratio of the local velocity V_w to the average $\langle V_w\rangle$ along the dimensionless sector length. Our 2D model predicts a uniform velocity, a trend also predicted by 3D CFD simulations. The most noticeable difference occur at the entrance of the sector where the flow is not yet fully established and bottom of the sector where is the filtration velocity is only 25% of the average velocity, whereas in the main part of the sector, the local velocity predicted by the 3D simulations is somewhat lower by 20%, which is left unexplained at this stage. Note that the filtration velocity along the sector length x, is a key element in the perspective of clogging simulations. From this

comparison we validate the assumption of a uniform filtration velocity through the media along the sector length.

The pressure drop through the filter media can also be estimated with our 2D model as well as the pressure drop in the inlet and outlet chambers. For the specified conditions, the pressure drop through the filter media is numerically evaluated at 3372 Pa (0.03372 bar). For comparison, the pressure drop in the inlet and outlet channels are respectively 48 Pa and 72 Pa. A key result is that the pressure drop through the filtration chambers is dominated by the pressure drop through the filtration media and not by the hydrodynamic through the chambers.

Also as discussed in previous works, (e.g. Gan and Allen, 1999; Koltuniewicz et al., 2004; Oxarango et al., 2004), it is important to realize that aiming at optimizing operating conditions or filter design, this simplified model is much easy to use for a parametric study than 3D CFD simulations that are less affordable in terms of computational time.

3. Clogging the filtration media

The development of a model for the clogging of filtration media begins with the consideration of two clogging mechanisms: surface blocking of media openings by particles, building of a cake on the top of the media. Because filtration media have a mesh geometry characterized by openings of constant section in the media thickness direction, we assume that depth blocking is negligible, a different case from non-woven fibrous media. Depth blocking may occur when particles with size smaller than opening size are caught on the inner walls of the openings due to specific adsorption or by flow constrictions.

Experiments including visualizations of particle capture are desirable for a better understanding of capture mechanisms. Such approaches are currently under development for model grids and monodisperse particles, (e.g. Psoch and Schiewer, 2006; Rebai et al., 2010). An alternative consists in carrying out filtration tests to measure the dynamics of pressure increase during a filtration and to compare with the prediction of clogging models representative for the aforementioned mechanisms. We thus carried out filtrations tests with a standardized dispersion, referred as with Arizona test fine sand (READE advanced materials USA), commonly used for tests in hydraulic fluid for in hydraulic, automotive, and aerospace applications.

3.1. *Surface blocking mode*

In this model, the fluid is supposed to contain suspended spherical solid particles with a size distribution in the range $[d_{pl} - d_{pu}]$. For Arizona test fine sand, the size distribution as well as the number of particles per unit volume is estimated for 16 classes between 4 μm and 70 μm as reported in Table 2. The screen media has characteristic opening size our mesh size d_h. We shall assume a mechanistic criterion for particle blocking: only the particles with equivalent diameter larger than the opening size d_h, are caught. Moreover, we consider each particle covers and completely clogs the opening. Aggregation of particles over time is not considered in this model. The initial number of openings n_o is calculated from geometrical screen area for one sector A_s, opening size d_h and hydraulic porosity ε of the screen by Eq. (23), noting that A_m the open surface of the screen media is equal to the product of A_s and d_h:

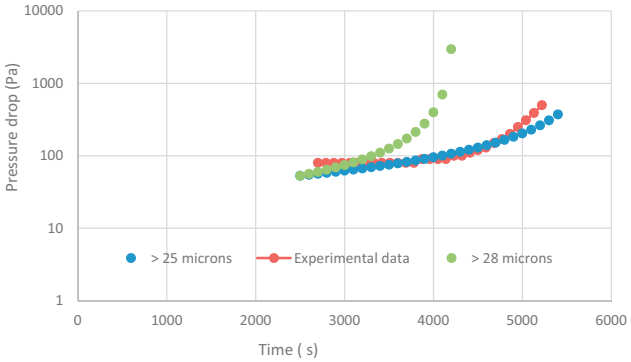

Fig. 5 – Variations of pressure drop versus filtration time: curves from top to bottom: numerical results assuming clogging by particles of minimal size 28 microns, data from experimental tests, numerical results assuming clogging by particles of minimal size 25 microns.

$$n_0 = \frac{A_s \varepsilon}{{d_h}^2} \tag{21}$$

If n_p is the total number of particles per unit volume of fluid of diameter larger than the mesh size d_h, that contribute to block the screen, the number $n(t)$ of outstanding openings at time t is given by:

$$n(t) = n_o - Q_s n_p t \tag{22}$$

where Q_s is the volumetric liquid flow rate in the sector.

The increase of the pressure drop due to the progressive clogging of openings by particles is then calculated from the following equation which refers to change in the number of openings with time:

$$\Delta P = \frac{\mu R n_0 Q_s}{A_s n(t)} \tag{23}$$

Inserting Eq. (22) into Eq. (23) yields the evolution of pressure drop for a sector as a function of time for the grid clogging model,

$$\Delta P = \frac{\mu R n_0 Q_s}{A_s \left(n_0 - \frac{Q_s}{A_s} n_p t\right)} \tag{24}$$

We have computed the evolution of pressure drop versus time using Eq. (24) assuming clogging of the mesh by particles of (i) size equal or larger to the mesh size (larger than 25 μm) (ii) larger than the mesh size (larger than 28 μm).

The volumetric liquid flow rate Q_s is equal to 1.09×10^{-5} m^3 s^{-1} and the fluid viscosity is 0.015 Pa s for a temperature of 40 °C. Fig. 6 shows the evaluation of pressure drop ΔP across a sector as a function of time during standardized filtration experiments using the Arizona fine sand dispersion t for a volumetric flow rate to 1.09×10^{-5} m^3 s^{-1}.

As can be seen from Fig. 5, the pressure drop evolution collapses reasonably well onto a single curve with the values predicted by the grid clogging model for a criteria based on *size equal or larger to the mesh size*. The results show an evolution in two main periods, namely a period of very moderate increase where the particles are progressively trapped at the surface of the openings followed by a

Table 2 – Size distribution of solid particles entering the filter expressed in terms of number of particles per 20 ml of fluid for 16 classes between 4 μm and 70 μm. Total mass concentration of particles is 3 mg l^{-1}.

Internal disk-type diameter (m)	External disk type diameter (m)	Number of sectors by element	Number of elements in the filter	Chamber half height (m)	Chamber length (m)	Hydraulic resistance of screen (m^{-1})	Absolute mesh size (μm)
0.078	0.150	8	16	0.007	0.065	47.6×10^5	25

period of sharp increase in pressure drop. When the time of operation exceeds a critical time of 4500 s, experimental data show that the pressure drop diverges toward values of about 400 Pa. Before that critical time, constant low pressure drop of about 80 to 90 Pa has been recorded in the test experiment. We can note that the model fits quite well the clogging time experienced in the test when taking into account the total number particles with nominal size larger than 25 μm entering the filter. We have plotted in Fig. 6, the variation of pressure drop as a function of the fraction of open holes using Eq. (22) to compute the fraction of open holes $n(t)/n_o$ versus time. We note that the sharp increase in pressure drop is correlated to a reduced fraction of open holes. We may assess that when the fraction of the remaining open holes is lower than a critical fraction of 10% then pressure drop diverges.

3.2. *Cake filtration mode*

In this model, we assume that the filter media is fouled by a layer of particles before all the holes are physically clogged. The pressure drop will then be preferentially related to the rate of cake growth described by a well-established cake-filtration model (Ting et al., 2006).

The pressure drop is computed as,

$$\Delta P = \mu\, Q_s\, (R^* + R_{ca}) \tag{25}$$

where μ is the fluid viscosity, Q_s is the flow rate in the sector, R^* is the resistance of the mesh sheet and R_{ca} the resistance of the cake, which is expressed as,

$$R_{ca} = \frac{e(t)}{k_{ca}} \tag{26}$$

where $e(t)$ is the cake thickness at time t of filtration.

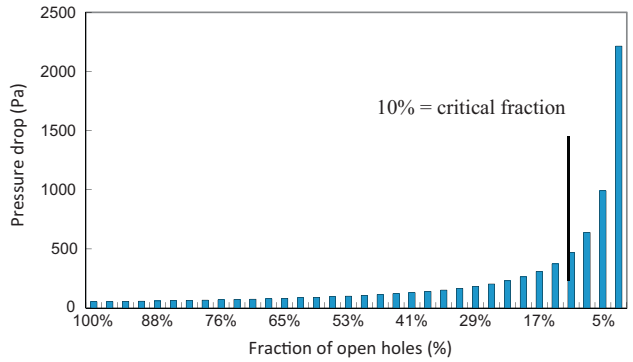

Fig. 6 – Pressure drop through the screen (numerical results) as a function of the fraction of free openings at the screen surface.

k_{ca} is the cake permeability, which is expressed by the classical Kozeny–Carman equation,

$$k_{ca} = \frac{\varepsilon_{ca}^3\, d_{pmoy}^2}{180\,(1-\varepsilon_{ca})^2} \tag{27}$$

where ε_{ca} is the cake porosity taken as equal to 0.36; d_{pmoy} is the average particle size calculated from the number n_{pi} of particles of size d_{pi} per unit volume of fluid.

$$d_{pmoy} = \frac{\sum_i n_{pi} d_{pi}^3}{\sum_i n_{pi} d_{pi}^2} \tag{28}$$

The evolution of cake thickness $e(t)$ as a function time can be deduced from the volume of particles captured at time t and is given by:

$$e(t) = \frac{\pi Q_s \sum_i n_{pi} d_{pi}^3 t}{6(1-\varepsilon_{ca})A_s} \tag{29}$$

Inserting Eqs. (26) and (29) into Eq. (25) gives the expression for the pressure drop for cake filtration model

$$\Delta P = \mu\, Q_s \left[R^* + \left(\frac{180\pi Q_s (1-\varepsilon_{ca}) \sum_i n_{pi} d_{pi}^3}{6 A_s \varepsilon_{ca}^3 d_{pmoy}^2} t \right) \right] \tag{30}$$

Fig. 7 presents the variations of pressure drop versus time obtained with the cake model. Eq. (30) predicts a linear variation of pressure drop with time, a very different feature from experimental data curve. Moreover the time necessary for clogging is very small: a few seconds compared to experimental time 4000 s. The pressure drop predicted by the cake

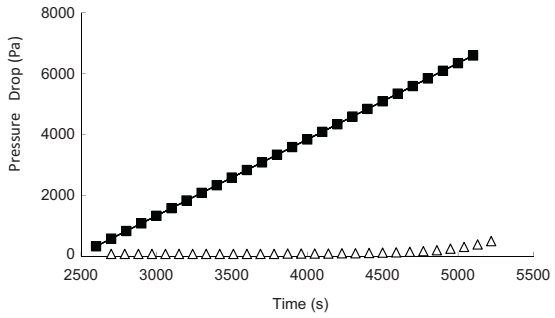

Fig. 7 – Variations of pressure drop though versus filtration time assuming cake growth at the surface of the screen: curve with black squares represents numerical results from cake filtration model, curve with empty triangles corresponds to experimental data from the test.

model after a filtration time of 4500 s is 42 times larger than the experimental value.

3.3. *Choice of a clogging model*

Based on the comparison of the predictions of the two models with experimental data, the conclusion is clearly that the most relevant model is the grid clogging model. Naturally, this model is based on simplifications like particles form factor and does not take into account the possible occultation of several pores by a single particle not the occurrence of particle aggregation. Note that we are mainly interested in the prediction of pressure drop, a key element in the multi-scale modeling we aim to develop. In that respect, we believe that the simplified grid clogging model is sufficient for this issue.

4. Modeling of stationary regime for an automatic self-cleaning filter

This section reports on the model we have developed to compute the pressure drop at the scale of the automatic self-cleaning filter.

One important parameter when operating such an automatic filter is the backflushing time The back-flushing time is the time between two consecutive shifts of the fluid distributor. At any time, there are always M sectors in filtration mode and 1 sector in back-flushing mode. We shall assume that the time required for a shift of the fluid distributor is very small compared with the back-flushing time.

In this model the impact of clogging on the pressure drop is described by the grid clogging model whereas the efficiency of the periodical backflushing is described through a parameter denoted α_b which represents the fraction of free openings just after backflushing period.

4.1. *Model development*

The primary objective of the model is to compute the evolution of pressure drop $\Delta P(t)$ as a function of the total volumetric rate entering the filter Q_f, the number of stacked elements N, the number of sectors $M+1$, the particle size distribution (or pollution profile) entering the filter, backflushing time t_b, mesh size d_h and screen area for one sector A_s. As mentioned before, the back flushing time is the time between two consecutive shifts of the fluid distributor. When the filter begins to operate or when there is a change in the operation conditions, there exists a transient period before reaching a stationnary regime, where the pressure drop across any particular sector varies periodically. In this work we focus on the stationnary regime. Only dimensional variables are used in this section.

We recall that we assume $M+1$ sectors with M the number of sectors in filtration mode. Note that owing to the design of disk type chamber, M has to be an odd number. The pressure drop is assumed to be the same through each element. Thus

$$\Delta P(t) \approx \Delta P_f(t) \approx \Delta P_{ei}(t) \quad 1 \le i \le N \tag{31}$$

where $\Delta P_f(t)$ and $\Delta P_{ei}(t)$ are the pressure drop across the whole filter and element i respectively. Suppose we start a cycle at time $t=0$, just after a shift of distributor and we want to compute the evolution of $\Delta P(t)$ from $t=0$ to $t=t_b$, i.e. just before a new shift of distributor (we recall that t_b is the backflushing time). We assume that sector #1 has just been backflushed at $t=0$. Thus sector M is the dirtiest at $t=0$.

Let α_{j0} be the fraction of free openings in the screen of sector j at $t=0 (1 \le j \le M)$.

We begin the analysis by expressing that the sum of flow rates through each sector in filtration mode should be equal to Q_f the total volumetric flow rate entering the filter.

$$Q_f = \sum_{j=1}^{M} Q_{sj} \tag{32}$$

where Q_{sj} is the flow rate in sector j.

Let n_o be the number of openings of the mesh, and suppose that there are now only n_t openings left, the others being blocked by particles. The average filtration velocity seen by the free opening is then given simply by

$$V_w(t) = V_{w0}/\alpha \tag{33}$$

where V_{w0} is the average filtration velocity when the mesh is clean and $\alpha = n_t/n_o$ (α is the fraction of free openings at time t). As a result, the pressure drop through the sector becomes

$$\Delta P = \alpha^{-1} \mu R V_{w0} = \alpha^{-1} \mu R \frac{Q_s}{2A_s} \tag{34}$$

The factor 2 in Eq. (34) comes from the fact that there are an upper and a lower filter media, each of area A_s, in each sector.

From this, Eq. (32) gives

$$Q_f = \frac{\Delta P(t) A_s}{\mu R} \sum_{j=1}^{M} \alpha_j = \frac{\Delta P(t) A_s}{\mu R^*} \Omega(t) \tag{35}$$

$$\Omega(t) = \sum_{j=1}^{M} \alpha_j \tag{36}$$

We express the evolution of α_j for each screen of each sector as

$$\frac{d\alpha_j}{dt} = -\frac{n_p}{n_0} \frac{Q_{sj}}{2} = -\frac{n_p A_s}{n_0 \mu R} \alpha_j \quad \Delta P \quad \text{with} \quad \alpha_j = \alpha_{j0} \quad \text{at} \quad t = 0 \tag{37}$$

where we recall that n_p is the number of particles of size greater than the screen opening size d_h per unit volume of fluid. Summing up the M Eq. (37) and using Eq. (36) lead to

$$\frac{d\Omega(t)}{dt} = -\frac{n_p}{2n_0} Q_f \tag{38}$$

which can be readily integrated to give

$$\Omega(t) = \Omega_0 - \frac{n_p Q_f}{2n_0} t \tag{39}$$

with $\Omega_0 = \sum_{j=1}^{M} \alpha_{j0}$.

Then we deduce from Eq. (34) an expression for the variation of pressure drop with time of operation

$$\Delta P(t) = \frac{\mu R Q_f}{2A_s} \frac{1}{\left(\Omega_0 - \frac{n_p Q_f}{2n_0} t\right)} \tag{40}$$

where the unique unknown is Ω_0.

In the following section, an expression for the calculation of Ω_0 is established

First we combine Eqs. (37) and (40) to yield, Eq. (41)

$$\frac{1}{\alpha_j}\frac{d\alpha_j}{dt} = -\frac{n_p Q_f}{2n_0}\frac{1}{\left(\Omega_0 - \frac{n_p Q_f}{2n_0}t\right)} \tag{41}$$

which can be integrated to give:

$$\alpha_j = \alpha_{j0}\left(1 - \frac{n_p Q_f}{2\Omega_0 n_0}t\right) \tag{42}$$

Finally, we express that the initial free opening fraction α_{j0} of sector j is equal to the free opening fraction in each screen of sector $j-1$ at time t_b (stationnary regime),

$$\alpha_{j0} = \alpha_{j-1}(t_b) \quad j = 2, M \tag{43}$$

with the additional condition that

$$\alpha_{10} = \alpha_b \tag{44}$$

where as mentioned before, α_b is the free opening fraction right after backflushing.

Combining Eqs (42) and (43):

$$\alpha_{j0} = \alpha_b\left(1 - \frac{n_p Q_f}{2\Omega_0 n_0}t_b\right)^{j-1} \quad j = 1,\ M \tag{45}$$

from which we get

$$\Omega_0 = \alpha_b\sum_{j=1}^{M}\left(1 - \frac{n_p Q_f}{2\Omega_0 n_0}t_b\right)^{j-1} \tag{46}$$

Solving for Ω_0 yields

$$\Omega_0 = \frac{n_p Q_f t_b}{2n_0}\frac{1}{\left[1 - \left(1 - \frac{n_p Q_f t_b}{2\alpha_b n_0}\right)^{1/M}\right]} \tag{47}$$

which can be used together with Eq. (40) to calculate the pressure drop where the unique parameter is α_b the free opening fraction right after backflushing.

For the parameter α_b, we can distinguish two situations:

- perfect cleaning, which corresponds to $\alpha_b = 1$. In this case at the end of backflushing period, all the particles have been removed and the number of apertures left open is equal to the initial one.
- imperfect (partial) cleaning. In this case, we shall assume that the backflushing time t_b is less than the time needed to remove all the particles from the mesh openings. In this case we developed an approach (see Annex I) to estimate $\alpha_b(t_b)$ the fraction of opening at the end of the backflushing period.

4.2. *Capabilities of the model*

4.2.1. *Influence of back flushing time and pollution concentration parameters*

To illustrate its capabilities, the model has been used to study the influence of backflushing time on Q_{sj}, the flow rate for each sector of an element. For these calculations, we used the same pollution profile data as used before, as well as the same geometrical and operating data. According to the above considerations, the reduced flow rate in each sector is given by,

$$\frac{Q_{sj}}{Q_f} = \frac{\alpha_b}{\Omega_0}\left(1 - \frac{n_p Q_f}{2\Omega_0 n_0}t_b\right)^{j-1} \tag{48}$$

We calculated the values of the reduced flow rates in the $M+1 = 8$ sectors of an element with the assumption of a perfect cleaning.

Results are reported in Fig. 8 for increasing backflushing time. The top curve shows the flow rate in sector #1, next curve below the flow rate in sector #2 and so on. As an example, we see that for t_b of the order or larger than 10 s, because sector #7 clogs during the back flushing period, the flow rate is reduced compared with average entrance flow rate, whereas the flow rate on sector #1 (just after the shift of distributor) is larger. For a backflushing time of 20 s we can estimate that the flow rate in sector #1 is 10% more than in sector #7. Of course the distribution of the flow over the different sectors of the element is a direct consequence of the distribution of the pressure drop in the different sectors: in sector #1, clogging has been removed so the pressure drop is low, whereas in sector #7, pressure drop progressively increases during the full rotation of the distributor.

We also calculated the values of the reduced flow rates in the $M+1$ sectors as a function of the pollution concentration. The concentration of solid particles per unit volume is expected to greatly influence the pressure drop in each sector. Results are reported in Fig. 9 for increasing pollution concentration. The influence of particle concentration is pretty much the same as for increasing the backflushing time. Again the distribution of the flow over the different sectors is related to the pressure drop in each sector a direct consequence of the number of particles per unit of volumetric

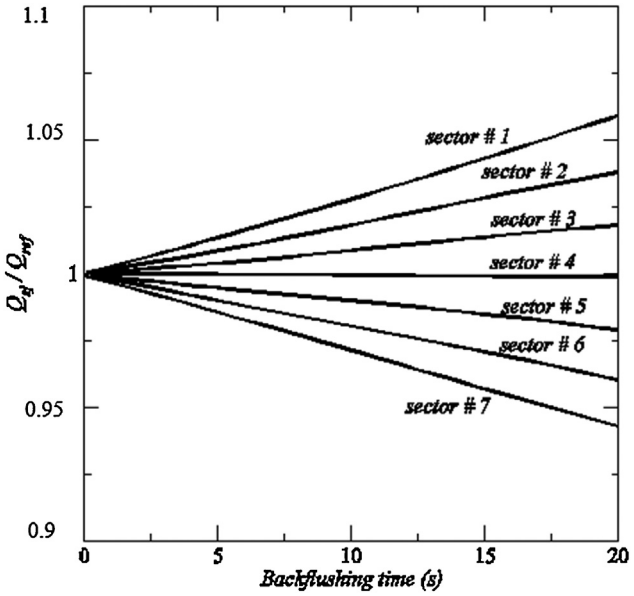

Fig. 8 – Specific load distribution rate ($m^3\ s^{-1}$) by sector versus backflushing period (s). The number of particles cm^{-3} greater than 25 μm in diameter is 60 particles cm^{-3}. The reference flow rate is $Q_s ref = 1.1 \times 10^{-5}\ m^3\ s^{-1}$.

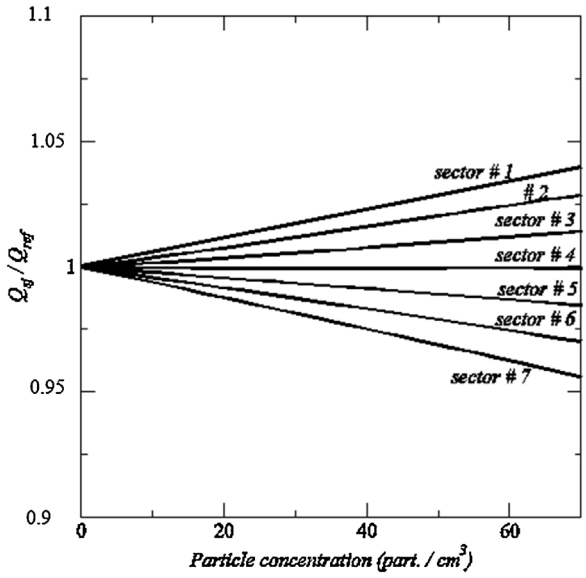

Fig. 9 – Specific load distribution (flow rate) for each sector as a function of the particle concentration (number of particles cm^{-3} greater than 25 μm in diameter; the pollution profile is similar for each concentration). The backflushing period is 15 s. The reference flow rate is $Q_s ref = 1.1 \times 10^{-5}\ m^3\ s^{-1}$.

flow rate (concentration) caught at the surface of the screen media. More simulation would be needed to determine critical backflushing time or critical particle concentration corresponding to a severe clogging of sector #7, sector #6, and sector #5, that would cause a drastic reduction of flow rate in these particular sectors. These critical parameters must be avoided because they correspond to situations for which only a fraction of the filter actually deliver a downstream flow. Since the purpose of this work is not a realistic optimization of a particular filter but an assessment of model capabilities, we did not investigate large range of parameter settings.

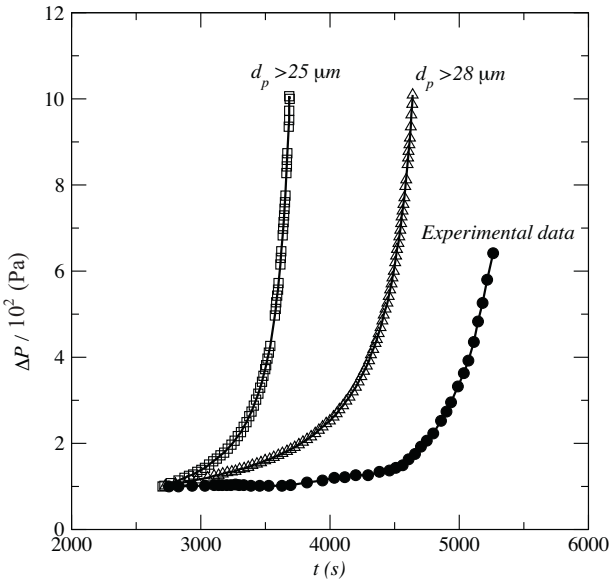

Fig. 10 – Pressure drop in the filter as a function of operation time: experimental data (black solid circles), numerical results assuming particles greater than or equal to 25 μm are caught (empty squares), numerical results assuming particles greater than or equal to 28 μm are caught (empty triangles).

4.2.2. *Pressure drop through the complete filter*

One capability of the model is to calculate the pressure drop at the scale of one-disc type element. Then using in a simple analytical up scaling procedure and assuming that the flow through each disc-type element is the same whatever the position of the element in the stack, one can estimate the evolution of pressure drop at the scale of the filter composed of N disc-type elements. Fig. 10 compares the calculations using geometrical data from Table 1 as well as date for the particle size distribution and operating conditions used in the previous section except for back-flushing time. The numerical and experimental data are compared for a back-flushing time of 3 s corresponding to an imperfect cleaning (α_b is almost equal to zero). This setting was chosen in order to be able to measure an increased pressure drop in an hour range. Realistic conditions with backflushing time of the order of 20 s would give an operating range of the order of several weeks. Two cases have been considered as far as particle filtration degree is concerned. The solid line with empty squares corresponds to results obtained assuming than particles of size greater than or equal to 25 μm are caught by the screen. The solid line with empty triangles corresponds to the results obtained assuming that the particles of size greater than or equal to 28 μm are caught by the screen.

As can be seen, the difference in time of clogging highlights the importance of the modeling of particle capture (specifically for particles close to the critical size). The good qualitative agreement with the experimental data however indicates that the main features of clogging at element scale are correctly taken into account in the model at the filter scale.

5. Conclusions

In this paper we presented an analytical model for stationnary (periodic) operating conditions of filtration and backflushing in an automatic filter. This model accounts for multi-scale and multi-physics considerations. We showed that the filtration velocity in a section of disc element, herein defined as a sector, can be considered as uniform for the typical conditions encountered in liquid filtration and that the 1D modeling correctly predicts the filtration velocity. We also concluded that the most relevant model is a screen clogging model for which the increase in pressure drop is related to the reduction of mesh free openings. We also developed a model to estimate the time needed for a sector to be correctly backflushed and defined as key parameter the free opening fraction of a sector after a given backflushing time.

The model was then used in a simple analytical upscaling procedure allowing to estimate the evolution of pressure drop at the scale of a filter element and deduce the time of clogging. Clogging scenario as a function of particle concentration and backflushing time were also investigated. A key result is that the longer the backflushing time, the larger the difference between the flow rates in each sector in the filter.

The model is based on several simplifying assumptions allowing one to develop quasi-analytical solutions. For this reason it greatly facilitates parametric studies as illustrated in this work. In addition to permit highlighting the main features of the automatic filter under normal operation conditions, the model can also serve as a basis for the development of more sophisticated models. Hence it opens up the route for

models aiming at optimizing the operation of the automatic filter and/or optimizing its design.

Acknowledgements

The authors are grateful to P. Schmitz for interesting discussions and to A. Ramadane for carrying out preliminary simulations.

Appendix A. Annex I: Modeling for the efficiency of the backflushing

The primary objective of the simplistic model is to calculate the fraction of apertures left open after a backflushing period $\alpha_b(t_b)$ depending on specified backflushing time and flow rate.

The backflushing model is based on the assumption that only a discrete number of particles block the filter media openings. This is of course consistent with the conclusion on the clogging model of the previous section. Here we suppose that n_p blocking particles are evenly distributed along the filter media. We consider again a 2D domain identical to the one considered in Section 2. The objective is to compute the exit time for each particle. The exit time is the time needed for a particle to travel from its initial position on the filter media to the entrance of the inlet chamber. The cleaning time t_c corresponds therefore to the exit time of the particle located initially the farthest from the entrance of the chamber section. When the backflushing time t_b is greater than or equal to the cleaning time, the backflushing operation may be considered as perfect since the filter media is perfectly clean at the end of backflushing. On the contrary, if the backflushing time is smaller than the cleaning time, a fraction of particles does not exit the inlet channel before the end of backflushing.

In accordance with the simulation presented in Section 2, the particles are supposed to follow the stream lines. If we know the velocity field (u, v) in the inlet chamber during backflushing, then the trajectory of a particle is given by solving the equations stating that Stokes number is much smaller than 1 ($St \ll 1$, no slip condition)

$$\frac{dx_p}{dt} = u; \quad \frac{dy_p}{dt} = v \tag{A-1}$$

where (x_p, y_p) are the dimensionless coordinates of the initial position of particle.

We checked the no slip conditions $St \ll 1$, assuming an average particle size of 4 μm, a particle density of 2500 kg m^{-3}, a fluid viscosity of 0.0255 Pa s, an average fluid velocity u in the chamber of 0.25 m s^{-1} and a characteristic length corresponding to L, the length of a chamber. The value of Stokes number defined as $\frac{\rho_p d_p^2 U}{\mu L}$ is equal to 5.10^{-6}.

Eq. (A-1) are solved using a fourth order Runge Kutta method. This gives the position of particle $(x_p(t), y_p(t))$ in the inlet chamber as a function of time. The particle exit time is obtained when $x_p = 0$ (entrance of the inlet chamber). Since the results reported in Section 2 indicate that the local velocity is quasi-uniform along the filter media (this also holds during backflushing), the velocity field can be determined analytically as before using the solution proposed in Koltuniewicz et al. (2004). This solution reads,

$$\frac{u(x,y)}{U_o} = \frac{3}{2}\frac{\langle u\rangle_y}{U_o}\left(1-y^2\right)\left[1-\frac{Re_w}{420}\left(2-7y^2-7y^4\right)\right]+O\left(Re_w^2\right)$$
$$\frac{v(x,y)}{U_o} = \frac{1}{2}\frac{Re_w}{Re_0}y\left(3-y^2\right)+\frac{Re_w^2}{Re_0}\left(\frac{1}{280}\left(-2y+3y^3-y^7\right)\right)+O\left(Re_w^3\right) \tag{A-2}$$

We recall that the origin of the coordinate system is at the center of the channel here (hence the filter media is at $y = 1$ and the center of chamber is at $y = 0$).

The average velocity $\langle u\rangle$ as a function of x is deduced from a simple mass balance, which gives a linear variation since the local filtration velocity is assumed to be uniform:

$$\langle u\rangle = U_0\left(1-\frac{hx}{L}\right) \tag{A-3}$$

Here as before U_0 is the average velocity in the inlet chamber section (U_0 is negative during back-flushing). For an illustration of the methodology, we choose the average velocity equal to 0.2488 m s^{-1} and the average filtration velocity $\langle V_w\rangle$ is equal to 0.0268 m s^{-1}. These inputs can easily be replaced with alternative data.

Fig. A.1a shows examples of particle trajectories in the inlet chamber for the 2D geometry, flow conditions and mesh characteristics detailed in Section 2. The channel being 65 mm long, it gives 2600 possible particle position along the filter cloth ($L/d_h = 2600$ for $d_h = 25$ μm). Fig. A.1b also shows the particle exit time as a function of particle initial position on the filter cloth. The exit time of the farthest particle is found to be 1.6 s for these conditions. However, most of particles exit the channel in less than 0.7 s. This is further illustrated in Fig. A.2 which shows the evolution of the number of particles m_p present within the channel during back-flushing as a function of time. We have assumed here that one particle was present on each mesh opening when back-flushing starts (thus leading to $m_{p0} = 2600$ particles initially). One can

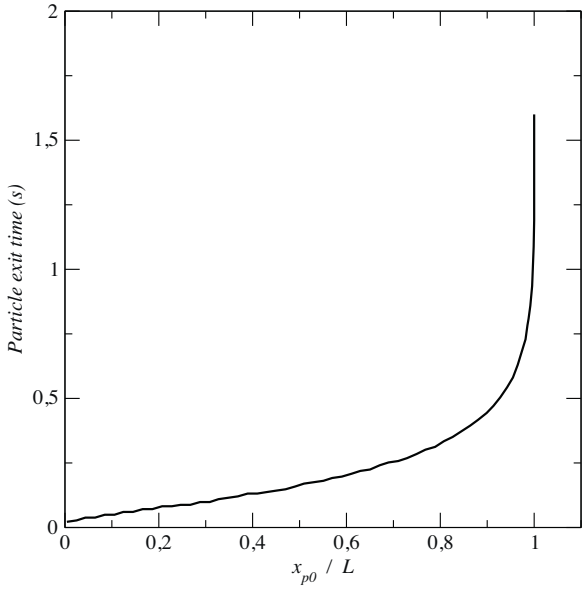

Fig. A.1 – (a) Examples of particle trajectories in the inlet channel during back-flushing. Note that y = 0 corresponds to the screen and y = 1 to inlet channel center in the figure. The arrow indicates the main direction of the flow in direction of channel entrance, (b) particle exit time as a function of particle initial position x_p0 on filter cloth.

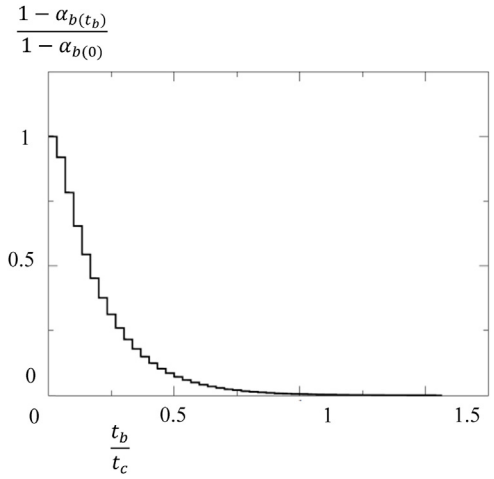

Fig. A.2 – Evolution of the number of particles present within the channel during backflushing as a function of time.

distinguish two phases: a first phase during which about 75% of the particles exit the domain, this takes about 0.3 s and a significantly longer tail during which the remaining particles exit.

As illustrated in Fig. A.2, we can deduce from this back-flushing model a functional relationship of the form:

$$\frac{1-\alpha_b(t_b)}{1-\alpha_b(0)} = f(t_b/t_c) = a_4(t_b/t_c)^4 + a_3(t_b/t_c)^3 + a_2(t_b/t_c)^2 + a_1(t_b/t_c) + a_0 \quad \text{(A-4)}$$

where t_b is the time of backflush and t_c the time needed to remove all the particles blocked on the opening (perfect cleaning) is equal for the flow conditions considered here to 1.6 s as shown on Fig. A.1b. The term $1-\alpha_b(0)$ in relation (A-4) represents the fraction of openings occupied by particles at the beginning of backflushing whereas $\frac{1-\alpha_b(t_b)}{1-\alpha_b(0)}$ is the fraction of particles still present at the end of back-flushing.

For a given flow rate entering the sector during the back flushing period, the backflushing efficiency can be estimated depending on two situations:

- full cleaning, which can be expected when $t_c < t_b$. Therefore $\alpha_b = 1$ is this case (mesh completely clean after back-flushing)
- imperfect (partial) cleaning when $t_c > t_b$. In this case, α_b can be estimated from the functional form of relation (A-4).

References

Ando, T., Akamatsu, K., Nakao, S., Fujita, M., 2012. Simulation of fouling and backwash dynamics in dead-end microfiltration: effect of pore size. J. Membr. Sci. 392, 48–57.

Bacchin, P., Marty, A., Duru, P., Meireles, M., Aimar, P., 2011. Colloidal surface interactions and membrane fouling: investigations at pore scale. Adv. Colloid Interface Sci. 164 (1), 2–11.

Benmachou, K., Schmitz, P., Meireles, M., 2003. Dynamic clogging of a pleated filter experimental and theoretical approaches for simulation. In: Anlauf, H., Schmidt, E. (Eds.), Proceedings of Filtech Europa Conference. Dusseldorf, Germany, pp. 51–57, vol. 2.

Berman, A.S., 1953. Laminar flow in channels with porous walls. J. Appl. Phys. 32, 1232.

Duignan, M.R., Nash, C.A., 2012. Experiments on cake development in crossflow filtration for high level waste. ASME J. Fluids Eng. 134 (8), 081302.

Gan, Q., Allen, S.J., 1999. Crossflow microfiltration of a primary sewage effluent–solid retention efficiency and flux enhancement. J. Chem. Technol. Biotechnol. 74, 693–699.

Koltuniewicz, A.B., Witek, A., Bezak, K., 2004. Efficiency of membrane-sorption integrate processes. J. Membr. Sci. 239, 129–141.

Li, H., Bertram, C.D., Wiley, D.E., 1998. Mechanisms by which pulsatile flow affects cross-flow microfiltration. AIChE J. 44 (9), 1950–1961.

Lin, J., Bourrier, D., Dilhan, M., Duru, P., 2009. Particle deposition onto a microsieve. Phys. Fluids 21, 073301–73311.

Oxarango, L., Schmitz, P., Quintard, M., 2004. Laminar flow in channels with wall suction or injection: a new model to study multi-channel filtration system. Chem. Eng. Sci. 59, 1039–1105.

Psoch, C., Schiewer, S., 2006. Resistance analysis for enhanced wastewater membrane filtration. J. Membr. Sci. 280, 284–297.

Rebai, M., Prat, M., Meireles, M., Schmitz, P., Baclet, R., 2010. A semi-analytical model for gas flow in pleated filters. Chem. Eng. Sci. 65, 2835–3284.

Ting, K.C., Wakeman, R.J., Nassehi, V., 2006. Modeling flow in monofilament filter cloths: Part 1—Prediction of pressure losse. Filtration 6 (2), 150–215.